Adsorption and Reaction of CO_2 on the RuO_2(110) Surface

Y. Wang, A. Lafosse, and K. Jacobi*

Department of Physical Chemistry, Fritz-Haber-Institut der Max-Planck-Gesellschaft, Faradayweg 4−6, D-14195 Berlin, Germany

Received: February 11, 2002; In Final Form: March 28, 2002

The interaction of CO_2 with the bare RuO_2(110) surface, exposing unsaturated Ru and oxygen atoms, was studied using high-resolution electron energy-loss spectroscopy (HREELS) and thermal desorption spectroscopy (TDS). At 85 K, CO_2 is found to adsorb only on coordinatively unsaturated Ru-cus sites giving rise to three different species: physisorbed CO_2, chemisorbed $CO_2^{\delta-}$, and $CO_2{\cdot}CO_2^{\delta-}$ dimers. A complete assignment of the vibrational spectra is reached which allows us to gain insight into the reactions involved. Upon annealing, two channels open up for physisorbed CO_2: desorption or further reaction with chemisorbed $CO_2^{\delta-}$ forming $CO_2{\cdot}CO_2^{\delta-}$ dimers. At 175 K, a bidentate carbonate is observed because of the reaction of $CO_2^{\delta-}$ with an O bridge. Further annealing induces a thermally activated conversion from the bidentate to a $CO_3^{\delta-}$ monodentate species. The latter is stable up to about room temperature and then decomposes into CO_2 and O_{ad}. The adsorption geometries of the different species are discussed in detail. The activation of CO_2 to form a chemisorption bond occurs only on the Ru-cus site. This gives further evidence for the key role played by Ru-cus in the catalytic activity of the bare RuO_2(110) surface.

1. Introduction

The interaction of CO_2 with metal and oxide surfaces is of importance in understanding a number of relevant surface catalytic processes on an atomic scale.[1,2] So far, the bonding, structure, and reactions of CO_2 adsorbed on single-crystal metal surfaces have been extensively studied.[3,4] However, less information is available on the interaction of CO_2 with well-characterized metal-oxide surfaces. The low electric conductivity of many oxides hinders the use of electron-spectroscopic methods. In recent years, this problem has been overcome by epitaxially growing thin oxide films on metal substrates.

In general, CO_2 exposure to oxide surfaces at low temperature leads to coexistence of two bonding states (see ref 3 and references therein): either physisorbed CO_2 may interact electrostatically with surface metal cations while keeping its linear configuration, or carbonate species may be formed via reaction with surface oxygen anions. Both adsorption states have been confirmed by ab initio calculations.[5−7] In addition, a chemisorbed CO_2 species, which is strongly bound with the metal cations in a bent geometry, was also reported on the reduced ZnO,[8,9] TiO_2,[10] and Cr_2O_3[11] single-crystal surfaces.

Recently, RuO_2(110) single-crystal surfaces have been produced by exposing Ru(0001) to high doses of O_2 at an elevated sample temperature.[12,13] The resulting surface, in the following noted as bare RuO_2(110) surface, is sketched in Figure 1. It is terminated by coordinatively unsaturated Ru (Ru-cus), coordinatively unsaturated bridge oxygen (O-bridge), and 3-fold coordinated layer oxygen (O-layer). This surface was found to exhibit high catalytic activity for CO oxidation even down to room temperature.[14,15] Furthermore, in a more recent study of the steady-state kinetics of CO oxidation, Wang et al.[16] showed that the so-called pressure and material gaps, found for Ru based catalysts, could be bridged realizing that the actual catalyst is RuO_2.

* To whom correspondence should be addressed. Phone: +49-30-8413-5201. Fax: +49-30-8413-5106. E-mail: jacobi@fhi-berlin.mpg.de.

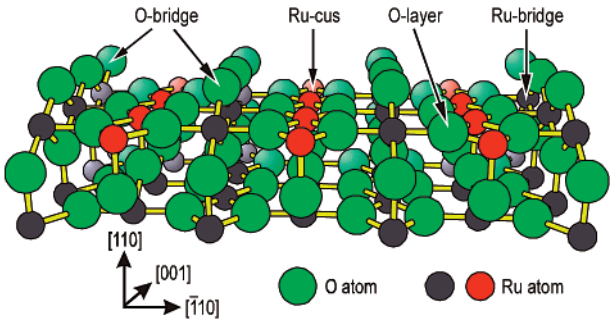

Figure 1. Ball-and-stick model of the bare RuO_2(110) surface in perspective view.

The present work is part of an enduring effort to evaluate the reactivity of the RuO_2(110) surface. Here we present data for CO_2 adsorption on the bare RuO_2(110) surface using high-resolution electron energy-loss spectroscopy (HREELS) and thermal desorption spectroscopy (TDS). We will show that at 85 K CO_2 adsorption takes place only on the Ru-cus sites. Three types of species can be identified: physisorbed CO_2, chemisorbed $CO_2^{\delta-}$, as well as $CO_2{\cdot}CO_2^{\delta-}$ dimers. We can further discriminate between two kinds of chemisorbed $CO_2^{\delta-}$ species, which further interact with CO_2 forming $CO_2{\cdot}CO_2^{\delta-}$ dimers upon annealing. Small amounts of carbonate are also found at a higher temperature. The identification of the above observed species allows us to gain some insight into the interaction of CO_2 with the RuO_2(110) surface. Geometric models of the respective adsorbate complexes will be proposed.

2. Experimental Section

The experiments were performed in an ultrahigh vacuum (UHV) apparatus consisting of two chambers separated by a valve.[17] The base pressure was 2×10^{-11} mbar. The upper chamber was used for sample preparation and contained facilities for thermal desorption spectroscopy (TDS), low-energy electron

10.1021/jp025619x CCC: $22.00
Published on Web 05/03/2002

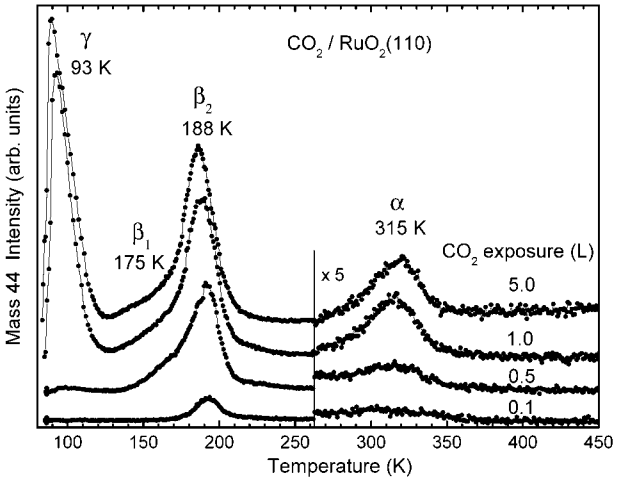

Figure 2. TD spectra of CO_2 (mass 44) for various CO_2 exposures in units of Langmuir (L) at 85 K on RuO_2(110). The heating rate was 3 K/s.

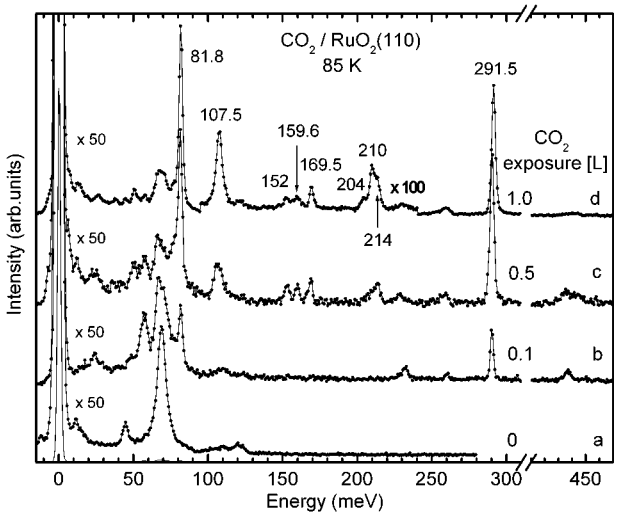

Figure 3. HREEL spectra for various CO_2 exposures at 85 K on RuO_2-(110). All spectra were recorded at 85 K in specular geometry with an incidence angle θ of 55° with respect to the surface normal, with an electron primary energy E_p of 3 eV and an energy resolution better than 2.5 meV.

diffraction (LEED), gas dosing, and surface cleaning by Ar ion sputtering. The lower chamber housed a HREEL spectrometer of the latest commercial Ibach design (Delta 0.5, SPECS, Germany). HREEL spectra were taken in specular geometry at an angle of incidence of 55° with respect to the surface normal. The primary electron energy was set to 3 eV, and the energy resolution was better than 2.5 meV.

The Ru(0001) surface was clamped between two Ta wires in narrow slits, could be heated by electron bombardment from the backside, and cooled to 85 K by liquid nitrogen; its temperature was measured with a Ni−CrNi thermocouple spot welded to the edge of the sample. Cleaning of the sample was achieved by repeated cycles of sputtering and annealing and checked by LEED and HREELS. The RuO_2(110) surface was prepared by exposing about 1×10^7 L of O_2 at a sample temperature of 700 K employing a glass capillary array doser directed toward the sample.[14,15] This procedure resulted in a surface which was covered by a thin single-crystalline layer of RuO_2(110) ordered in patches of three different domains, rotated laterally by 120°[12,13] as checked by LEED. The preparation could be repeated after restoring the original Ru(0001) surface by sputter-annealing.

The gas purity for CO_2 was 99.995%, and exposing was performed by backfilling the preparation chamber. Exposures are given in units of Langmuir (L) ($1\ L = 1.33 \times 10^{-6}$ mbar s).

3. Results

3.1. TD Spectra. In Figure 2, TD spectra of CO_2 (mass 44) are shown for different exposures at 85 K. At low CO_2 exposures, two broad desorption peaks are observed at around 188 and 315 K, respectively. With increasing CO_2 exposure, new peaks appear at lower temperatures. At an exposure of 1.0 L CO_2, the TD spectrum exhibits the following four peaks: γ-CO_2 (93 K), β_1-CO_2 (175 K), β_2−CO_2 (188 K), and α-CO_2 (315 K). For exposures larger than 1 L, the TD spectra remain unchanged meaning that the CO_2 adsorption is saturated at 85 K and that a CO_2 multilayer is not formed. The TD spectra of CO_2 suggest the presence of different CO_2 species which are identified in the following HREELS experiments. Assuming a preexponential factor of 10^{13} s^{-1} in first-order kinetics, we can obtain an activation energy of 25 kJ/mol for the desorption of γ-CO_2, revealing a weak bonding of this species. In a similar way, for α-CO_2, the activation barrier for a below identified decomposition process can be estimated to be 80 kJ/mol.

3.2. HREEL Spectra. *3.2.1. Adsorption of CO_2 at 85 K.* Figure 3 shows a set of HREEL spectra as a function of CO_2 exposure at 85 K. The observed energies and mode assignments for the different adsorption states are summarized in Table 1. The bare RuO_2(110) surface displays vibrational losses at 14, 45, 69, 109, and 120 meV (curve a), among them the most intense peak at 69 meV has been assigned to the stretching mode of O-bridge against the surface.[13] The peaks at 14 and 45 meV are likely to be due to phonons, but a calculation of the phonon spectrum is still missing. The peaks at 109 and 120 are assigned to atoms of minor coordination, e.g., at the domain boundaries, because the losses decrease in intensity for better prepared surfaces.

After each CO_2 exposure at 85 K, the RuO_2 peaks decreases in intensity as explained by screening through CO_2. Simultaneously, two new leading peaks appear at 81.8 and 291.5 meV. They are characteristic for physisorbed CO_2 and assigned to the degenerate bending (δ) and the asymmetric stretching (ν_a) mode, respectively. In the energy range of the symmetric stretching vibration, two weak features are clearly observed at 159.6 and 169.5 meV and attributed to a Fermi resonance between the symmetric stretching (ν_s) and the first overtone ($\delta^{(2)}$) of the bending mode.[18] All these losses are in excellent agreement with the gas-phase values (82.7, 159.3, 172.1, and 291.3 meV)[18,19] demonstrating that CO_2 is very weakly adsorbed and maintains its linear geometry. Thus, γ-CO_2 is identified as linear, physisorbed CO_2.

For higher exposures, the spectra display additional weak losses at 50.5, 107.5, 152, and 210 meV (see curve d) which can be assigned to chemisorbed CO_2 by comparison with the characteristic stretching modes of CO_2 in transition-metal complexes[20−25] observed in the 136−151 and 194−221 meV energy regions. The chemisorption of CO_2 is generally connected with the formation of an anionic molecule: $CO_2^{\delta-}$. In addition, a weak feature observed at 204 meV suggests the existence of another chemisorbed species. A further loss is observed at 214 meV which is the dominant mode in this energy region for an exposure of 0.5 L CO_2 (curve c). It may be due to another CO_2 species as substantiated by the annealing

TABLE 1: Vibrational Energies [meV] and Mode Assignments for Physisorbed CO_2, Chemisorbed $CO_2^{\delta-}$, Dimerized $CO_2 \cdot CO_2^{\delta-}$, and Reacted $CO_3^{\delta-}$ Carbonate, all adsorbed on the Bare $RuO_2(110)$ Surface[a]

modes	CO_2 gas phase[b]	CO_2 phys.	$CO_2^{\delta-}$ (I)	$CO_2 \cdot CO_2^{\delta-}$ (I)	$CO_2^{\delta-}$ (II)	$CO_2 \cdot CO_2^{\delta-}$ (II)	$CO_3^{\delta-}$ (I)	$CO_3^{\delta-}$ (II)
T_z			50.5	51	50.5	51.5		
δ	82.7	81.8	107.5	81.8	107.5	82		84
				106		108.6		
ω^-	159.3	159.6		160		160		
ω^+	172.1	169.5		169		169		
$\delta^{(2)}$		163.6[c]						
ν_s		165.5[c]			152	151.5	123	150
ν(C−O)			152	152.5				
ν(C═O)			210	214			197	
ν_{as}	291.3	291.5		291	204	207	151.5	173
						290.7		

[a] The vibrational modes are denominated as: T, translational mode; δ, in-plane bending mode; ν_s and ν_{as}, symmetric and asymmetric stretching modes; ω^- and ω^+, Fermi dyad due to resonance between ν_s and $\delta^{(2)}$ (overtone of δ); ν(C−O), C−O stretching mode; ν(C═O), C═O stretching mode. [b] References 18 and 19. [c] Calculated values.

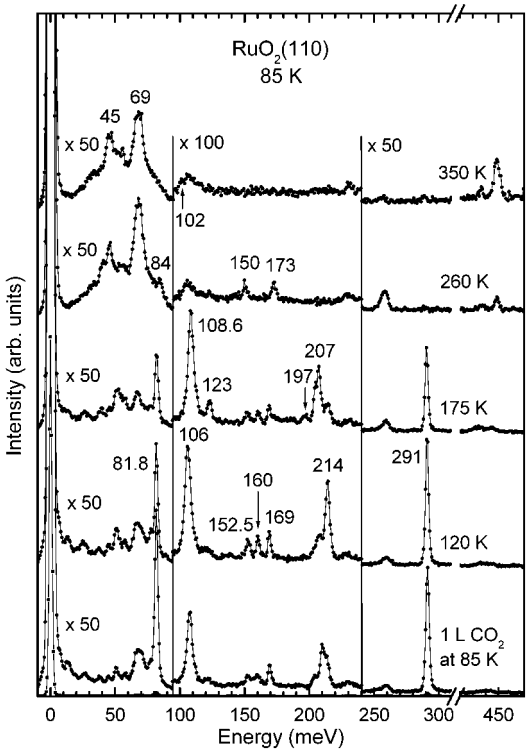

Figure 4. HREEL spectra for an exposure of 1 L CO_2 on $RuO_2(110)$. After exposure at 85 K, the sample was subsequently annealed to the indicated temperatures. Parameters as for Figure 3.

experiments shown below. All of these losses will be discussed in detail and assigned below.

In addition, other less-intensive peaks are observed. The losses at 26, 58, 231, 437, and 448 meV are assigned to a H_2O-like species which results from hydrogen adsorption on O-bridge.[26] Also, a small amount of CO, adsorbed on Ru-cus sites, is visible as supported by the ν(Ru−CO) and ν(C−O) modes at 38 and 259 meV.[15] At 85 K these losses increase with collection time of the HREEL spectra and, we conclude, therefore, that they originate from adsorption of hydrogen and CO from the residual gas, which cannot be avoided for the reactive $RuO_2(110)$ surface even at a background pressure of 3×10^{-11} mbar.

3.2.2. HREELS after Annealing to Higher Temperatures. The sample was exposed to 1 L CO_2 at 85 K and subsequently annealed to the temperatures indicated in Figure 4. The respective HREEL spectra were measured at 85 K. After annealing to 120 K, the losses at 204 and 210 meV have disappeared, whereas the mode at 214 meV gains in intensity and the peak at 107.5 meV shifts to 106 meV. It is surprising that the unperturbed CO_2-related modes are still present, whereas at this temperature, the desorption of γ-CO_2 is completed (see Figure 2). This observation can be interpreted as being due to the formation of $CO_2 \cdot CO_2^{\delta-}$ dimers in which the linear CO_2 molecule is weakly bound via its carbon atom to an oxygen atom of the chemisorbed $CO_2^{\delta-}$ species. Besides the major dimer species $CO_2 \cdot CO_2^{\delta-}$ (I), a new feature is observed at 207 meV which becomes the dominant mode after heating the sample to 175 K. Simultaneously, the peak at 214 meV has lost largely in intensity, and the loss at 106 meV shifts to 108.6 meV, implying the formation of another dimer species $CO_2 \cdot CO_2^{\delta-}$ (II) as supported by the observation of the unperturbed CO_2-related modes. The β_1-CO_2 state at about 175 K in TDS is therefore associated with CO_2 desorption from the $CO_2 \cdot CO_2^{\delta-}$ (I) dimer.

In addition, after annealing to 175 K, the spectrum displays two new weak features at 123 and 197 meV which cannot be attributed to a $CO_2^{\delta-}$ species. The observation of the mode at 123 meV suggests the formation of a carbonate species $CO_3^{\delta-}$ (I), because a peak in the energy region 120−135 meV is only found for carbonate[27] and serves, therefore, to distinguish it from $CO_2^{\delta-}$. Upon heating to 260 K, $CO_2 \cdot CO_2^{\delta-}$ (II) species disappear completely, corresponding to the β_2−CO_2 state in TDS, whereas new modes at 84, 150, and 173 meV evolve. They can be assigned to another carbonate species $CO_3^{\delta-}$ (II). A transformation between the two types of carbonate species seems to occur as supported by the disappearance of the $CO_3^{\delta-}$ (I) related losses and the much higher decomposition temperature. The vibrational and structural properties of the two carbonate species will be discussed in more detail in section 4.4.

During further annealing to 350 K, the carbonate related losses disappear which reveals that the carbonate decomposes into O_{ad} and CO_2. The latter is not stable at this temperature and desorbs immediately as characterized by the α-CO_2 desorption peak. As a result, the CO_2 desorption rate is controlled by the decomposition step and exhibits first-order character in TDS. Note that α-CO_2 may also partly originate from the reaction of CO from residual gas and O-bridge which should take place at about 300 K.[15] In addition, the decomposition of the "H_2O-like" species is observed as indicated by the appearance of OH related peaks at 55 and 448 meV.[26]

4. Discussion

The TDS and HREELS results, presented so far, reveal that CO_2 adsorption on the bare $RuO_2(110)$ surface is very complex. CO_2 exposure at 85 K and annealing to higher temperatures result in the observation of different species, whose vibrational and geometric properties will be discussed in detail in this

section. A complete assignment of the vibrational spectra makes it possible to gain insight into the reaction processes involved. The influence of the structural and electronic properties of the RuO_2(110) surface will also be discussed.

4.1. Physisorbed CO_2. Physisorption of CO_2 has been often reported on metal and oxide surfaces (see ref 3 and references therein); however, less information is available concerning the Fermi resonance of physisorbed CO_2. Recently, Krenzer et al.[28] have verified the presence of the Fermi resonance for physisorbed CO_2 on a Ag(110) surface precovered by CO_3. For the linear CO_2 molecule, the Fermi resonance occurs because the symmetric stretching mode ν_s is energetically nearly degenerate with the overtone $\delta^{(2)}$ of the bending mode and both are of the same symmetry (Σ_g^+ state).[18] As a consequence, they split into two perturbed modes, the so-called Fermi dyad, which is clearly observed here on the bare RuO_2(110) surface at 159.6 and 169.5 meV. Because of a strong mixing of the eigenfunctions of both unperturbed modes, the two observed losses can no longer be unambiguously identified as $\delta^{(2)}$ and ν_s, respectively.

On the basis of first-order perturbation theory, the frequencies of the Fermi dyad are given by[18,28]

$$\omega^{\pm} = \bar{\omega} \pm \frac{1}{2}\sqrt{4W^2 + \Delta^2} \qquad (1)$$

where $\bar{\omega} = (1/2)(\delta^{(2)} + \nu_s)$, W is the Fermi constant, and $\Delta = \nu_s - \delta^{(2)}$. Taking the anharmonic term of the CO_2 potential into account, one obtains an overtone excitation with frequency[29]

$$\omega^{(2)} = 2\omega^{(1)} - 2\omega_e\chi_e \qquad (2)$$

where $\omega^{(1)}$ is the measured fundamental frequency, ω_e is the fundamental frequency calculated in the harmonic approximation, and χ_e is the anharmonicity parameter. The latter was found to be on the order of 10^{-3} for CO_2 in the gas phase[30,31] as well as for CO_2 adsorbed on Ag(110).[28] Assuming the same value of χ_e for CO_2 on RuO_2(110), the anharmonicity correction in (2) can be neglected within our energy resolution. Thus, from (1) and the observed losses, we can calculate the energies for $\delta^{(2)}$ and ν_s (both unperturbed) to be 163.6 and 165.5 meV, respectively (Table 1). ν_s is higher than $\delta^{(2)}$ in agreement with the assignment for CO_2 adsorbed on Ag(110),[28] whereas in the gas phase, $\delta^{(2)}$ is slightly above ν_s. The energy shift produced by the perturbation is dependent on Δ, the separation of the unperturbed levels. For the fully degenerate states ($\Delta = 0$), the shift is largest reflecting the exact resonance. It was found to be 6 meV in the gas phase with $\Delta = 0.7$ meV,[19,31] whereas in our case, the shift decreases to 4 meV because of the larger splitting of the unperturbed levels with $\Delta = 1.9$ meV. In addition, the Fermi constant W is given by the anharmonic term in the potential energy and is determined here to 4.9 meV. This value is smaller than the gas-phase value of 6.1 meV indicating a relative weak interaction between the unperturbed levels. In addition, the intense δ and ν_{as} peaks demonstrate that both modes are dipole active, revealing that physisorbed CO_2 is oriented on RuO_2(110) with its molecular axis tilted with respect to the surface normal.

4.2. Chemisorbed CO_2: $CO_2^{\delta-}$. It is well-known from the literature that chemisorbed CO_2 exhibits completely different vibrational properties compared to physisorbed CO_2. The dramatic downshift of the stretching energy from 291 to about 210 meV, upon CO_2 chemisorption, suggests a reduced bond order for the chemisorbed state, which is connected with the formation of a bent $CO_2^{\delta-}$ species. This configuration can be explained by the Walsh diagram[32] of CO_2 which shows that the energy of the unoccupied, doubly degenerate $2\pi_u$ molecular orbitals shifts by 2 eV to higher binding energy in going from the linear (180°) to the bent (130°) conformation, making the former $2\pi_u$ orbitals suitable for bonding with other molecular orbitals of the same symmetry. As a consequence, CO_2 chemisorption involves charge transfer from the substrate to the molecule and gives rise to a $CO_2^{\delta-}$ anionic species. Ab inito calculations[33] for gas-phase CO_2^- radicals have revealed that the potential energy minimum of CO_2^- with a bent angle near 135° lies below that of linear CO_2.

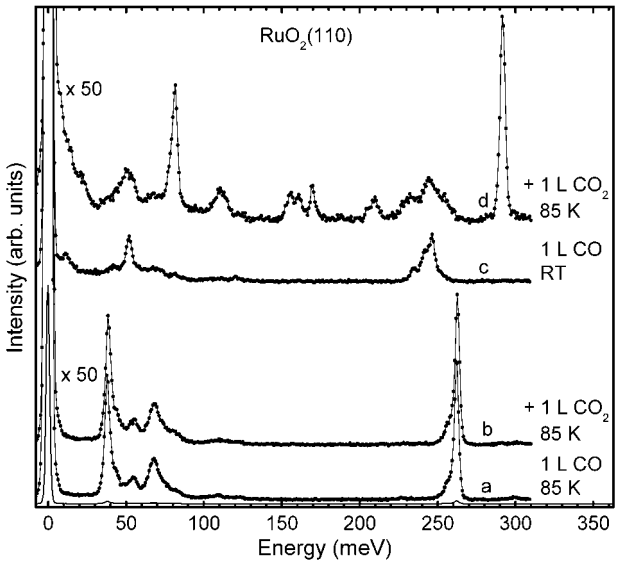

Figure 5. HREEL spectra for differently prepared and reacted RuO_2-(110) surfaces. The sample was exposed to (a) 1 L CO at 85 K and then (b) 1 L CO_2 at 85 K; (c) 1 L CO at room temperature and then (d) 1 L CO_2 at 85 K. Parameters as for Figure 3.

Generally, at low temperatures, adsorption of CO_2 on metal oxide surfaces leads to the formation of carbonate species via reaction of CO_2 with surface oxygen. Indeed, we have observed carbonate instead of $CO_2^{\delta-}$ species on an O-rich RuO_2(110) surface[34] after exposing CO_2 at 85 K. The O-rich surface can be prepared by exposing O_2 to the bare surface resulting in a weakly bound atomic oxygen on top of Ru-cus.[13,15] On the bare RuO_2(110) surface, on the other hand, one would expect carbonate formation to occur at O-bridge.

To determine on which site CO_2 is adsorbed, we have performed the following experiment: the Ru-cus atoms were first capped by CO molecules through exposure of 1 L CO at 85 K,[15] as demonstrated by the ν(Ru−CO) and ν(C−O) modes of CO-cus at 38 and 262 meV (curve a in Figure 5); when this surface was further exposed to 1 L CO_2 (curve b in Figure 5), no CO_2 related modes were observed. That means that at 85 K CO_2 adsorption needs empty Ru-cus sites to take place, that CO_2 does not interact with O-bridge, and in particular that there is no carbonate formation which was expected above for more general arguments. This conclusion is further confirmed by the next experiment: first, by exposing 1.0 L CO at room temperature so that the O-bridge species is removed via the reaction with CO (curve c in Figure 5), a reduced RuO_2(110) surface was prepared. The Ru-bridge sites freed from O-bridge are capable of bonding CO. Thus, CO is adsorbed at the Ru-bridge sites giving rise to the ν(Ru−CO) mode at 52 meV as well as ν(C−O) modes at 234, 242, and 246 meV.[14,15] After reduction of the surface by reaction with CO, the sample was cooled to 85 K and then exposed to 1.0 L CO_2. The corresponding HREEL spectrum (curve d in Figure 5) exhibits nearly the same vibrational losses as observed for CO_2 on the bare

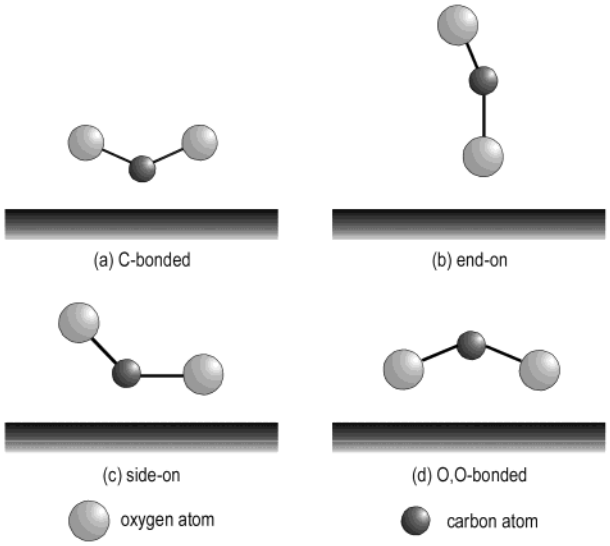

Figure 6. Schematic representation of different types of coordination for CO_2 chemisorbed on a surface: (a) C-bonded, (b) end-on, (c) side-on, and (d) O+O coordination.

TABLE 2: Coordination Modes and Observed Stretching Vibrational Energies [meV] of CO_2 in Transition-Metal Compounds

mode of coordination	ν(C═O) or ν_{as}(OCO)	ν(C−O) or ν_s(OCO)	$\Delta\nu$
end-on[a]	213−221	142−151	62−79
C-coordination[b]	194−207	147−150	44−60
side-on[c]	201−216	137−149	57−73

[a] Reference 22. [b] References 22 and 24. [c] References 20−23 and 25.

surface (see Figure 4). We conclude therefore that the observed peaks at 51, 108, 152, 204, and 210 meV are attributed to chemisorbed $CO_2^{\delta-}$ and not to carbonate.

Taking into account the required charge transfer from the metal cation to CO_2, the formation of $CO_2^{\delta-}$ species on oxide surfaces is in general energetically unfavorable. However, the Ru-cus cations on the bare RuO_2(110) surface are coordinatively unsaturated exposing a kind of dangling bond.[12] Their positive charge is reduced as compared to the Ru cations in the bulk. This enables Ru-cus to provide electrons to CO_2 to initiate chemisorption leading to a bent $CO_2^{\delta-}$ anion. The fact that the activation of CO_2 occurs only on the Ru-cus site gives further evidence for the key role played by the latter in the catalytic activity of the RuO_2(110) surface.[12,14,15]

Now we focus on the adsorption geometry of the bent $CO_2^{\delta-}$. As shown in Figure 6, a chemisorbed CO_2 may assume the following orientations relative to the surface: (a) C-coordination (C-bonded), (b) O-coordination (end-on), (c) mixed C+O-coordination (side-on), and (d) O+O-coordination (O,O-bonded). For the end-on and side-on structures, the two oxygen atoms are no longer equivalent, and the CO bond (of CO_2) near to the surface becomes a single C−O bond. The configuration of the chemisorbed species may be derived from the comparison of the observed frequencies with the spectroscopic data of CO_2 in transition-metal compounds,[20−25] for which it is known that there exist three types of structures displaying different stretching energies as listed in Table 2.

The energy of the stretching modes as well as the magnitude of their splitting are related to the bonding geometry of CO_2. An end-on geometry should give a structure with a larger OCO angle,[25] i.e., a less bent coordinated CO_2 because of a reduced π back donation compared to the two other structures. This

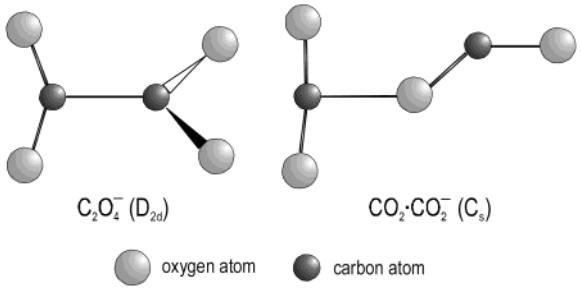

Figure 7. Schematic representation of the two stable structures for the $(CO_2)_2^-$ dimer anion with the corresponding symmetries:[35] (a) $C_2O_4^-$ (D_{2d}) and (b) $CO_2{\cdot}CO_2^-$ (C_s).

induces a stretching mode ν(C═O) with higher energy (213−221 meV) and a largely reduced bending mode δ(OCO) as found, e.g., at 89 meV for a $CuCO_2$ complex.[22] Obviously, we can rule out this possibility.

The comparison of the measured vibrational energies with those listed in Table 2 shows that an assignment of the major chemisorbed state $CO_2^{\delta-}$ (I) to a side-on configuration (C_s symmetry) is reasonable. Thus, the observed peaks at 50.5, 107.5, 152, and 210 meV can be attributed to the frustrated translation perpendicular to the surface $T_\perp$(Ru−CO_2), the bending mode δ(OCO), the stretching modes ν(C−O), and ν(C═O), respectively. The high-lying bending mode is also in good agreement with that at about 105 meV in the CO_2 transition-metal compounds.[20] The intensity of the ν(C−O) mode is low because the C−O bond is oriented nearly parallel to the surface, and the dipole moment perpendicular to the surface is therefore small.

The weak feature at 204 meV indicates the existence of a minority species $CO_2^{\delta-}$ (II). Its bending and low-lying stretching modes are not resolved from those of the major species $CO_2^{\delta-}$ (I). It may be assigned to a $CO_2^{\delta-}$ in C coordination (type a in Figure 6) because of the small splitting (52 meV) of the stretching modes. This configuration was also proposed for TiO_2 powder[10] giving IR peaks at 151 and 203 meV. For a $CO_2^{\delta-}$ species in C coordination with C_{2v} symmetry, i.e., with its molecular axis perpendicular to the surface, only three modes involving T_z, δ, and ν_s are dipole active. The appearance of the asymmetrical stretching mode at 204 meV proves a reduced symmetry of $CO_2^{\delta-}$ which should be adsorbed on Ru-cus in a tilted geometry.

4.3. Dimer: $CO_2{\cdot}CO_2^{\delta-}$. According to the ab inito calculations[35] two stable structures for the $(CO_2)_2^-$ dimer anion were found (Figure 7): the D_{2d} -symmetric $C_2O_4^-$ in which the electron is shared equally between the two CO_2 groups and an asymmetric $CO_2{\cdot}CO_2^-$ anion complex (T-shaped) with C_s symmetry in which the electron is essentially located on one of the CO_2 molecules. The D_{2d} structure is slightly lower in energy than the C_s structure. Both forms have been observed in a solid neon matrix,[36,37] and the asymmetrical stretching modes at 230 and 206.5 meV are characteristic for $C_2O_4^-$ dimer and the CO_2^- group in the $CO_2{\cdot}CO_2^-$ dimer, respectively. However, not much is known about the structural and vibrational properties of $(CO_2)_2^{\delta-}$ dimers adsorbed on metal or oxide surfaces, till now.

The present annealing experiments reveal the existence of a $CO_2{\cdot}CO_2^{\delta-}$ dimer on the bare RuO_2(110) surface, which is formed via the reaction of a $CO_2^{\delta-}$ anion with CO_2:

$$CO_2^{\delta-}\text{ (I)} + CO_2 \rightarrow CO_2{\cdot}CO_2^{\delta-}\text{ (I)} \quad (3)$$

$$CO_2^{\delta-}\text{ (II)} + CO_2 \rightarrow CO_2{\cdot}CO_2^{\delta-}\text{ (II)} \quad (4)$$

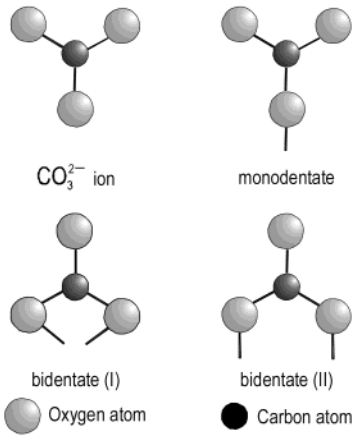

Figure 8. Schematic representation of the types of coordination for carbonate formed on a surface: (a) CO_3^{2-} ion, (b) monodentate, (c) bidentate (I), and (d) bidentate (II).

TABLE 3: Stretching Energies [meV] of Carbonate Adsorbed on Oxide Surfaces in Different Coordinations[27a]

coordination	ν_1	ν_2	ν_3
CO_3^{2-} ion	126.5−135		176−180
monodentate	129−134	161−170	182−190
bidentate (I)	126.5−128	155−158	190−201
bidentate (II)	121.5−126.5	151−158	201−207

[a] Depending on the coordination of the carbonate, ν_1, ν_2, and ν_3 can be further distinguished as follows: CO_3^{2-} ion: $\nu_1 - \nu_s$, $\nu_3 - \nu_{as}$; monodentate: $\nu_1 - \nu$(C−O), $\nu_2 - \nu_s$, $\nu_3 - \nu_{as}$; bidentate: $\nu_1 - \nu_s$, $\nu_2 - \nu_{as}$, $\nu_3 - \nu$(C═O).

Thus, upon annealing, two channels open up for physisorbed CO_2: desorption or reaction with chemisorbed $CO_2^{\delta-}$. In the dimer, the neutral CO_2 moiety is basically undistorted and interacts very weakly with the Ru-cus atoms as demonstrated by the typical losses at 81.8, 160, 169, and 291 meV which are in good agreement with the gas phase values. It is also weakly bound via the carbon atom to an oxygen atom of the chemisorbed $CO_2^{\delta-}$ in the dimer in a T-shape geometry (see Figure 7). Upon dimer formation, a blueshift is observed for the $CO_2^{\delta-}$ part: from 210 to 214 meV for dimer I and from 204 to 207 meV for dimer II. This reflects the weak coupling between the $CO_2^{\delta-}$ and CO_2 moieties in the dimer as confirmed by the theoretical calculation.[35] A slight blueshift of about 1 meV compared with isolated CO_2^- was also determined in a neon matrix.[36,37] The relatively high stability of the $CO_2 \cdot CO_2^{\delta-}$ dimer is consistent with the theoretical study which suggested that $CO_2 \cdot CO_2^{\delta-}$ is more stable by 0.9 eV than the $CO_2^{\delta-}$ monomer[3] because of the relatively large quadrupole moment of CO_2 (−3.2 au).[38] Finally, we note that, upon annealing, the intensity of the 214 meV loss decreases and that of the 207 meV increases. The latter indicates to our belief that, besides desorption, dimer I is partly transferred into dimer II.

4.4. Carbonate: $CO_3^{\delta-}$. As shown in Figure 8, four types of coordination are reported for carbonate species formed at a surface exhibiting different stretching energies[27] reported as ν_1, ν_2, and ν_3 in Table 3. The free carbonate ion is of planar symmetry and its asymmetric stretching mode ν_3 is doubly degenerate. In the case of a monodentate or bidentate, the symmetry of the group is decreased causing the ν_3 vibration to split into two components. The degree of splitting depends on the type of coordination and the ionic-covalent character of the metal−oxygen bond.[27,39] The splitting is larger for the bidentate than for monodentate, as reflected in metal−carbonate complexes[40] in which the separation of the two stretching modes is only about 19 meV for monodentate but over 40 meV for bidentate. Furthermore, the amount of splitting increases with increasing covalency of the metal−oxygen bond (i.e., with a decrease of the effective negative charge of the oxygen ion) and has been found to be about 70 meV in covalently bonded organic carbonates.[40] In addition, parameters such as the O−C−O angle and the metal−oxygen bond length also affect the splitting but to a much lesser degree as proven by the calculations.[41]

By comparison of the observed carbonate vibrational energies with the data listed in Table 3, it is clear that the $CO_3^{\delta-}$ (I) species observed after annealing at 175 K is associated with a bidentate coordination, and the losses at 123 and 197 meV are thus attributed to the stretching modes ν_s(OCO) and ν(C═O), respectively. The asymmetric stretching mode ν_{as}(OCO) may be not resolved from the ν_s(OCO) mode of $CO_2^{\delta-}$. For the other carbonate species, $CO_3^{\delta-}$ (II), formed at 260 K, the configuration of a bidentate can be ruled out because of the absence of a peak near 200 meV. The small splitting of the two losses in the energy region 150−180 meV reveals that the monodentate form becomes the preferred species which gives rise to the δ(OCO) in-plane bending mode at 84 meV and the ν_s(OCO) and ν_{as}(OCO) stretching modes at 150 and 173 meV, respectively. These modes are also observed with much larger intensity on the O-rich RuO_2(110) surface and are further confirmed as carbonate species by isotopic substitution measurements.[34] In addition, the out-of-plane bending mode π(OCO) is expected to appear at 100−110 meV;[40] however, the present loss at 106 meV rather originates from some surface defect because its intensity remains constant after carbonate decomposition at 350 K. The monodentate stretching mode ν(C−O) is not observed, and this may be explained by its much smaller intensity compared to the ν_s(OCO) and ν_{as}(OCO) modes as supported by the IR spectra of the cobalt (III) carbonate complexes.[42] The observation of the asymmetric stretching mode and the absence of the π(OCO) mode indicate that the carbonate plane is perpendicular to the surface but with a tilted $RuO-CO_2$ axis.

Finally, we discuss the reaction mechanism of carbonate formation. It is known[41] that on polycrystalline oxide surfaces carbonate species are produced via reaction of CO_2 with the surface basic centers, i.e., oxygen anions in low-coordination states, where the basicity represents the ability of the surface oxygen to donate charge to the adsorbate. The bare RuO_2(110) surface provides coordinatively unsaturated anions (O-bridge) and the reaction occurs most likely as follows:

$$CO_2 \cdot CO_2^{\delta-} \rightarrow CO_2^{\delta-} + CO_2\uparrow \quad (5)$$

$$CO_2^{\delta-} + \text{O-bridge} \rightarrow CO_3^{\delta-}\text{ (I)} \quad (6)$$

where the $CO_3^{\delta-}$ (I) species is bicoordinated to both a Ru-bridge cation and a Ru-cus cation, resulting in a bidentate (II) structure. That this reaction did not take place at 85 K can be explained by its relative high activation barrier. Further annealing induces a thermally activated conversion from the bidentate $CO_3^{\delta-}$ (I) to the monodentate $CO_3^{\delta-}$ (II), the latter is stable up to about room temperature and decomposes completely after heating to 350 K:

$$CO_3^{\delta-} \rightarrow O^{\delta-} + CO_2\uparrow \quad (7)$$

The appearance of O-cus as demonstrated by the ν(Ru−O) mode at 102 meV implies that the monodentate carbonate can be bonded to Ru-cus as well as to Ru-bridge.

In addition, another possible reaction pathway was suggested on metal surfaces,[43−45] involving the disproportionation of a

$CO_2 \cdot CO_2^{\delta-}$ dimer:

$$CO_2 \cdot CO_2^{\delta-} \rightarrow CO_3^{\delta-} + CO \quad (8)$$

As shown in Figure 4, the CO related losses are observed at 38 and 259 meV. However, they result most likely from CO adsorbed from the residual gas rather than from the disproportionation of $CO_2 \cdot CO_2^{\delta-}$ dimers, because they are observed for all spectra in Figure 4 and gain in intensity with the collection time and with increasing the number of free Ru-cus sites. Furthermore, after removing most O-bridge species, the CO_2 desorption peak at 315 K is strongly reduced in intensity, indicating that the surface oxygen, O-bridge, is necessary for the carbonate formation on the $RuO_2(110)$ surface. Therefore, this reaction pathway, carbonate formation via dimer disproportionation, can be excluded.

5. Conclusion

The interaction of CO_2 with the bare $RuO_2(110)$ surface at 85 K is of complex nature leading to the coexistence of physisorbed CO_2, chemisorbed $CO_2^{\delta-}$, and $CO_2 \cdot CO_2^{\delta-}$ dimer species. Despite the very involved HREEL spectra, all energy-loss peaks could be assigned in a consistent manner. A complete assignment of the vibrational spectra allows us to gain insight into the reaction processes involved.

At 85 K, the first incoming CO_2 molecules interact only with the Ru-cus sites leading to physisorption as well as chemisorption underlining the reactivity of the Ru-cus sites. Upon annealing, these states can further interact forming $CO_2 \cdot CO_2^{\delta-}$ dimers. At 175 K, a bidentate carbonate is formed via reaction of $CO_2^{\delta-}$ with O-bridge and a thermally activated conversion from the bidentate to the monodentate $CO_3^{\delta-}$ species takes place with further annealing. The latter is stable up to about room temperature and then decomposes into CO_2 and O_{ad} species. The adsorption geometries of the different species are discussed in detail. Some geometry parameters could be derived from the vibrational spectra.

Acknowledgment. We thank Professor G. Ertl for support and P. Geng for technical assistance. Fruitful discussions with Dr. Jinhai Wang and Chaoyang Fan are acknowledged. Y.W. thanks the German Academic Exchange Service (DAAD) for a stipend.

References and Notes

(1) Kiselev, V. K.; Krilov, O. V. *Adsorption and Catalysis on Transition Metals and their Oxides*; Springer: Heidelberg, 1989.
(2) Kung, H. H. *Transition Metal Oxides: Surface Chemistry and Catalysis*; Elsevier: Amsterdam, 1989.
(3) Freund, H.-J.; Roberts, M. W. *Surf. Sci. Rep.* **1996**, *25*, 225.
(4) Solymosi, F. *J. Mol. Catal.* **1991**, *65*, 337.
(5) Pacchioni, G. *Surf. Sci.* **1993**, *281*, 207.
(6) Pacchioni, G.; Ricart, M.; Illas, F. *J. Am. Chem. Soc.* **1994**, 116, 10152.
(7) Melle-Franco, M.; Pacchioni, G.; Chadwick, A. V. *Surf. Sci.* **2001**, *478*, 25.
(8) Göpel, W.; Bauer, R. S.; Hansson, G. *Surf. Sci.* **1980**, *99*, 138.
(9) Møller, P. J.; Komolov, S. A.; Lazneva, E. F.; Pedersen, E. H. *Surf. Sci.* **1995**, *323*, 102.
(10) Rasko, J.; Solymosi, F. *J. Phys. Chem.* **1994**, *98*, 7147.
(11) Seiferth, O.; Wolter, K.; Dillmann, B.; Klivenyi, G.; Freund, H.-J.; Scarano, D.; Zecchina, A. *Surf. Sci.* **1999**, *421*, 176.
(12) Over, H.; Kim, Y. D.; Seitsonen, A. P.; Wendt, S.; Lundgren, E.; Schmid, M.; Varga, P.; Morgante, A.; Ertl, G. *Science* **2000**, *287*, 1474.
(13) Kim, Y. D.; Seitsonen, A. P.; Wendt, S.; Wang, J.; Fan, C.; Jacobi, K.; Over, H.; Ertl, G. *J. Phys. Chem. B* **2001**, *105*, 3752.
(14) Fan, C. Y.; Wang, J.; Jacobi, K.; Ertl, G. *J. Chem. Phys.* **2001**, *114*, 10058.
(15) Wang, J.; Fan, C. Y.; Jacobi, K.; Ertl, G. *Surf. Sci.* **2001**, *481*, 113.
(16) Wang, J.; Fan, C. Y.; Jacobi, K.; Ertl, G. *J. Phys. Chem. B* **2002**, *106*, 3422.
(17) Shi, H.; Jacobi, K.; Ertl, G. *J. Chem. Phys.* **1993**, *99*, 9248.
(18) Herzberg, G. *Infrared and Raman Spectra*; Van Nostrand: New York, 1945.
(19) Rothman, L. S. *Appl. Opt.* **1986**, *25*, 1795.
(20) Aresta, M.; Nobile, C. F. *J. Chem. Soc., Dalton Trans.* **1977**, 708.
(21) Aresta, M.; Nobile, C. F. *Inorg. Chim. Acta* **1977**, *24*, L49.
(22) Mascetti, J.; Tranquille, M. *J. Phys. Chem.* **1988**, *92*, 2177.
(23) Jegat, C.; Fouassier, M.; Mascetti, J. *Inorg. Chem.* **1991**, *30*, 1521.
(24) Jegat, C.; Fouassier, M.; Tranquille, M.; Mascetti, J. *Inorg. Chem.* **1991**, *30*, 1529.
(25) Jegat, C.; Fouassier, M.; Tranquille, M.; Mascetti, J.; Tommasi, I.; Aresta, M.; Ingold, F.; Dedieu, A. *Inorg. Chem.* **1993**, *32*, 1279.
(26) Wang, J.; Fan, C. Y.; Jacobi, K.; Ertl, G. in preparation.
(27) Davydov, A. A. *Infrared Spectroscopy of Adsorbed Species on the Surface of Translation Metal Oxides*; John Wiley & Sons: Chichester, U.K., 1990.
(28) Krenzer, B.; Constant, L.; Conrad, H. *J. Chem. Phys.* **1999**, *111*, 1288.
(29) Ibach, H. *Electron Energy Loss Spectroscopy and Surface Vibrations*; Academic: New York, 1982.
(30) Chedin, A. *J. Mol. Spectrosc.* **1979**, *76*, 430.
(31) Suzuki, I. *J. Mol. Spectrosc.* **1968**, *25*, 479.
(32) Rabalais, J. W.; McDonald, J. M.; Scherr, V.; McGlynn, S. P. *Chem. Rev.* **1971**, *71*, 73.
(33) Carmichael, I.; Bentley, J. *J. Phys. Chem.* **1985**, *89*, 2951.
(34) Lafosse, A.; Wang, Y.; Jacobi, K. *J. Chem. Phys.* Submitted.
(35) Fleischman, S. H.; Jordan, K. D. *J. Phys. Chem.* **1987**, *91*, 1300.
(36) Jacox, M. E.; Thompson, W. E. *J. Chem. Phys.* **1989**, *91*, 1410.
(37) Zhou, M.; Andrews, L. *J. Chem. Phys.* **1999**, *110*, 6820.
(38) Hirschfelder, J. O.; Curtiss, C. F.; Bird, R. B. *Molecular Theory of Gases and Liquids*; Wiley: New York, 1954.
(39) Hair, M. L. *Infrared Spectroscopy in Surface Chemistry*; Marcel Dekker: New York, 1967.
(40) Little, L. H. *Infrared Spectra of Adsorbed Species*; Willmer Brothers Ltd.: London, 1966.
(41) Davydov, A. A.; Shepotko, M. L.; Budneva, A. A. *Kinet. Catal.* **1994**, *35*, 272.
(42) Gatehouse, B. M.; Livingstone, S. E.; Nyholm, R. S. *J. Chem. Soc.* **1958**, 3137.
(43) Freund, H.-J.; Messmer, R. P. *Surf. Sci.* **1986**, *172*, 1.
(44) Kiss, J.; Revesz, K.; Solymosi, F. *Surf. Sci.* **1988**, *207*, 36.
(45) Solymosi, F.; Klivenyi, G. *Surf. Sci.* **1994**, *315*, 255.